









# Selective Antimicrobial Properties of W-Ge Nanocomposite Thin Films

S. Atasoy<sup>1\*</sup> , Y. Kurul<sup>1</sup> , S. Aktas<sup>1</sup> , F. Sarcan<sup>2</sup> , M. S. Kurt<sup>3</sup> , A. Ayna<sup>4</sup> , E. Darendelioğlu<sup>4</sup> ,  
and A. Erol<sup>2</sup> 

<sup>1</sup>Giresun University, Faculty of Engineering, Department of Mechanical Engineering, 28200, Giresun, Türkiye

<sup>2</sup>Istanbul University, Faculty of Science, Department of Physics, Vezneciler, 34134, Istanbul, Türkiye

<sup>3</sup>Erzurum Technical University, Science Faculty, Department of Fundamental Science, 25050, Erzurum, Türkiye

<sup>4</sup>Bingöl University, Faculty of Science and Literature, Department of Chemistry, 12000, Bingöl, Türkiye

## ABSTRACT

The antimicrobial properties of W-Ge nanocomposite thin films as a function of Ge concentration were investigated within the scope of this study. The films were deposited on an AZ61Mg substrate using a magnetron sputter source with a co-deposition technique. Structural analyses showed that all coatings had a composite crystal structure. Additionally, the morphological investigation indicated that films had goosefoot-type structures at low Ge concentrations (5% and 10%), while Ge-rich films (40% and 60%) had cauliflower-type structures. The 20% Ge concentration coating had both structures. Regarding the surface morphology, the root mean square roughness of the surface reached its maximum value at a Ge concentration of 60% while the surface roughness and wettability of all the films showed an opposite trend. The antimicrobial activity of the W-Ge nanocomposite films against gram-negative (*Salmonella typhimurium* NRRLE 4413, *Escherichia coli* ATCC 25922) and gram-positive (*Staphylococcus aureus* 6538 P, *Bacillus subtilis* IM 622) bacteria was investigated via disc diffusion antibiotic sensitivity assay. Based on the antibacterial activity test, it was concluded that although all the films had antimicrobial efficiency against gram-negative and gram-positive bacteria, they were more effective against gram-positive bacteria. Moreover, with the increased surface roughness of the films, the number of grain boundaries, which cause an increase in the intensity of the oxide phases of the metals, increases, resulting in better antibacterial activity.

**Keywords:** nanocomposite thin film – tungsten – germanium – antibacterial efficiency – surface roughness

## 1. INTRODUCTION

Metallic composite thin films find extensive application across various fields such as environmental sensing, gas sensing, and water purification due to their enhanced performance, extended functionality as well as low cost, and given performance not attainable with bulk materials (Martin 2009; Zboun et al. 2020). Additionally, there are several studies focusing on the antimicrobial efficiency of metallic composite thin films. For instance, Menazea & Awwad (2020) reported on the antimicrobial efficiency of TiO<sub>2</sub> doped ZnO thin film, which was produced by pulsed laser ablation in liquid. Chuang et al. (2017) studied the effects of Ag<sub>2</sub>O on the antibacterial efficiency of ZnO/Ag<sub>2</sub>O composite thin film produced via magnetron sputtering method. Furthermore, Jena et al. (2020) presented a work that focused on the antibacterial properties of ternary composite coatings (graphene oxide - chitosan-silver) produced by the electrophoretic deposition technique. Arslan et al. (2022) reported on the antibacterial properties of Ge-DLC (diamond-like carbon) coatings produced by co-deposition technique via

magnetron sputtering method. As pointed out in various studies, the quality of the metallic composite materials, which depends on the growing method, has a significant effect on the sensing performance of the devices and/or functionalization of the material against bacteria. The most preferred thin film deposition techniques include physical and chemical vapour deposition, solution processes, and fusion processes (Voevodin et al. 1999; Somogyvári et al. 2012; Park et al. 2006; Helmersson et al. 2006; Roy et al. 2015; Sarcan 2020). Among these, the magnetron sputtering method allows the co-deposition of two metals by controlling the deposition rate under high-vacuum conditions, thereby avoiding any contamination.

The antimicrobial properties of Ge and its compounds were proved in a study on human pathogenic bacteria (Sellappa & Jeyaraman 2011). The studies on *Pseudomonas aeruginosa* planktonic and *Staphylococcus aureus* in suspension revealed that elemental Ge has antimicrobial activities (Kurt et al. 2021; Khalid et al. 2014). Ge naturally exists in very low concentrations in dairy foods. This metal, which is taken at a low amount

Corresponding Author: S. Atasoy E-mail: selcuk.atasoy@giresun.edu.tr

Submitted: 28.04.2023 • Revision Requested: 22.05.2023 • Last Revision Received: 29.05.2023 • Accepted: 05.06.2023 • Published Online: 12.06.2023



This article is licensed under a Creative Commons Attribution-NonCommercial 4.0 International License (CC BY-NC 4.0)

(0.4 - 3.4 mg) by the human body on a daily basis, contributes to controlling important biological functions such as maintaining sodium, potassium, glucose, and pH levels in balance, as well as lowering blood pressure (Okada et al. 1989; Nagata et al. 1985; Lück et al. 1999; Kaplan et al. 2004; Bian et al. 2017). A long period (18 months) of GeO<sub>2</sub> intake has been reported to result in acute renal failure in the human body due to the high dose intake (600 mg per day) (Nagata et al. 1985). Another study indicated that a patient who consumed 76 g of elemental Ge for 6 months developed renal failure (Lück et al. 1999). Bian et al. (2017) published a study on MgGe alloys, in which the potential cytotoxic effects of Ge on the human body were explored (Ge concentrations below 3wt percent). Their study demonstrated that MgGe alloys own excellent cytocompatibility, histocompatibility, good mechanical features, and corrosion resistance. The combination of such properties makes Ge metal and its alloys excellent potential candidates for implant materials. Moreover, the superior mechanical and physical qualities of W, such as its high melting point, wear resistance, and hardness, make it a desirable metal for use in a variety of applications.

In this study, we aim to obtain a composite of these two metals to enhance their superior properties against bacteria. For this purpose, W-Ge nanocomposite films as a function of Ge concentrations were deposited on AZ61Mg by magnetron sputtering approach to investigate their antibacterial efficiency in biological applications. Subsequently, the phase structure, surface morphology and wettability of the samples were examined. The antibacterial efficiency of W-Ge nanocomposite thin films as a function of Ge concentrations against gram-negative (*Salmonella typhimurium* NRRLE 4413, *Escherichia coli* ATCC 25922) and gram-positive (*Staphylococcus aureus* 6538 P., *Bacillus subtilis* IM 622) bacteria has been investigated.

## 2. EXPERIMENTAL DETAILS

### 2.1. Sample Preparation

Initially, AZ61 Mg substrates with dimensions of 10×20×2 mm were polished with 800–2000 mesh Silicon Carbide (SiC) abrasive papers, and 5 μm aluminium oxide (Al<sub>2</sub>O<sub>3</sub>) powder. Afterwards, then the surfaces of the Mg substrates were cleaned using an RCA type wet-cleaning procedure using acetone, methanol, and distilled water, respectively, in an ultrasonic cleaner for 3 minutes for each Mg substrate. The cleaning procedure was completed by blow-drying with nitrogen gas.

### 2.2. Thin Film Deposition

Tungsten (W) and Germanium (Ge) solid targets with a purity of 99.99% were used to coat Mg substrates. Plasma cleaning was applied to each target for 10 minutes prior to the coating process to remove contamination and achieve a more efficient

surface activity. All Mg substrates were coated using a Nanovak magnetron sputter system (Model: NVTS-400). The base pressure of the system was approximately  $4 \times 10^{-6}$  mTorr and the working pressure during the deposition process of all samples was approximately  $3 \times 10^{-3}$  mTorr. The co-deposition technique was used to deposit W-Ge nanocomposite coatings on the Mg substrates through the alteration of Ge concentration (5%, 10%, 20%, 40%, and 60%). A quartz thickness monitor was used to determine the deposition rates of the alloy samples. Ge concentrations of W-Ge nanocomposite coatings were controlled by adjusting the deposition rates of W and Ge based on the published work by Kurt et al. (2021). The distance between the substrate and the targets was approximately 15 cm, and the deposition was performed at room temperature. The thickness of the films was measured as  $1 \pm 0.9$  μm using an optical profilometer.

### 2.3. Sample Characterisation

The phase composition of the W-Ge nanocomposite coatings was analysed using the X-ray diffraction (XRD) technique with a Rigaku SmartLab diffractometer and a Cu Kα (1.5406 Å) radiation source. The morphology of the films at different Ge concentrations was evaluated using scanning electron microscopy (SEM) with an FEI Versa 3D Dual Beam. The surface roughness of the films was determined by atomic force microscopy (AFM – Park System XE-100E). The thickness of the films for each deposition condition was measured using a Bruker-Contour GT 3D Optical profilometer. The wettability and contact angle values of the coatings were analysed using the sessile drop technique with a contact angle goniometer (CAG) (Dataphysics OCA 15EC) at room temperature. The contact angle values were measured 60 seconds after pure water was dropped onto the surfaces.

### 2.4. In-vitro Bacterial Test

The antimicrobial activity of W-Ge nanocomposite coatings against gram negative (*Salmonella typhimurium* NRRLE 4413, *Escherichia coli* ATCC 25922) and gram-positive bacteria (*Staphylococcus aureus* 6538 P., *Bacillus subtilis* IM 622) was investigated via disc diffusion antibiotic sensitivity assay in which 6 mm of diameters discs were placed on the plates. The antibiotic discs and the Mg substrates which were coated with approximately 1 μm of W-Ge nanocomposite films at different concentration of Ge (5-60%) were placed on Muller-Hinton agar (MHA) plates inoculated with 100 μl of  $1 \times 10^6$  bacterial suspensions. Plates were then incubated at 37 °C overnight, followed by measurement of the diameters of inhibition zones. During the tests, an antibiotic mixture (penicillin-streptomycin) was used as a positive control.

### 3. RESULT AND DISCUSSION

Figure 1 displays the crystallographic properties of W-Ge nanocomposite films deposited on AZ61Mg by magnetron sputtering.  $2\theta$  Mg peak values of  $32^\circ.33$ ,  $34^\circ.66$ ,  $36^\circ.82$ , and  $48^\circ.13$  matched with the entry number of 96-151-2519, are observed due to the Mg substrate for all Ge concentrations. Crystal structure of  $\text{GeO}_2$  are observed at  $34^\circ.22$  with (111) plane from all coatings and at  $62^\circ.63$  with (221) planes from 20% and 60% Ge concentration. Additional  $2\theta$   $\text{GeO}_2$  peak is detected at  $72^\circ.73$  with (112) orientation from 5%, 40% and 60% coatings (entry no: 96-152-5833).  $2\theta$  peak values  $39^\circ.90$ , and  $57^\circ.70$  indicate the metallic W with the (101), (200) planes, respectively (entry no: 96-151-2550). Besides,  $\text{WO}_3$  crystal structure is obtained from all coatings at  $63^\circ.44$ , indicating the (400) plane. Whilst,  $2\theta$   $\text{WO}_3$  peak value of  $40^\circ.38$  with (201) plane is observed for 20% and 40% Ge concentrations, this is obtained at  $57^\circ.98$  with (202) plane for 60% Ge concentration (entry no: 96-100-4057). It can be concluded that the film coatings were formed as a composite crystal structure.

Figure 2 displays the morphology of the W-Ge nanocomposite thin films as a function of Ge concentrations. SEM images reveal two types of morphology, including goosefoot-type and

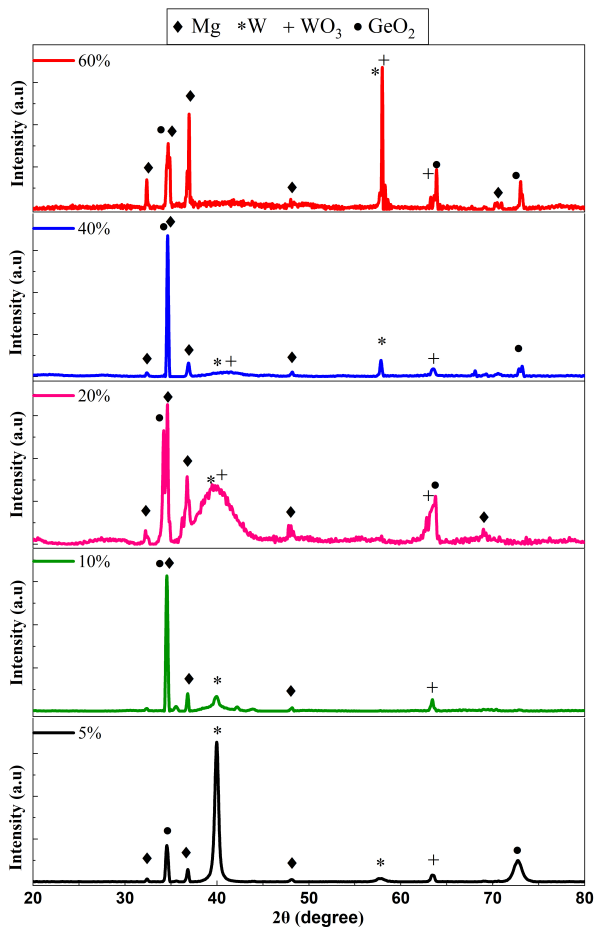


Figure 1. XRD spectrum of W-Ge thin film deposited on AZ61 Mg.

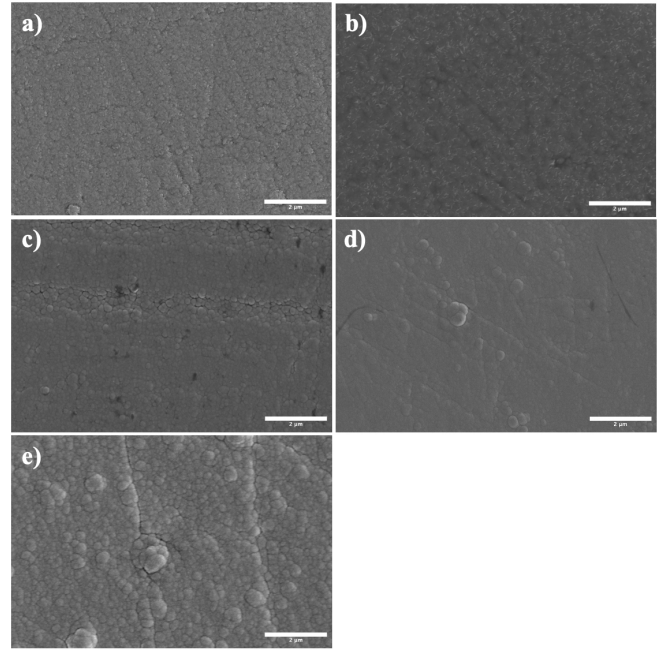


Figure 2. SEM images of the W-Ge nanocomposites coatings for a) 5% b) 10% c) 20% d) 40% e) 60% Ge concentrations.

cauliflower-type, for low (5%, 10%, 20%) and high Ge (40% and 60%) concentrations, respectively. In light of these morphological differences in the SEM images, it can be considered that there are two types of mechanisms in film formation. The increase of the Ge concentration for low Ge films led to a reduction in the goosefoot structure as shown in Figure 2a-c, which result in a reduction in the number of grains. However, the film with a 20% Ge concentration has a combined morphological structure of a goosefoot and a cauliflower-type. Conversely, coatings with high concentrations of Ge exhibit a contrasting effect, resulting in a cauliflower-like surface morphology in Ge-rich films. Specifically, the coating with a Ge concentration of 60% demonstrates a notable abundance of grains, as displayed in Figure 2e. The surface roughness of W-Ge nanocomposite coatings was evaluated using by AFM as a function of Ge concentration. It is found that the roughness varies between 35 to 90 nm, as illustrated in Figure 3a.

The surface roughness of W-Ge nanocomposite films at low Ge concentrations (5%, 10% and 20%) increase as a function of Ge concentration. This result is in a good agreement with SEM analyses since the surface morphology of thin film is less smooth and has some pores at 20% Ge concentration. Besides, surface roughness of 40% Ge concentration of W-Ge nanocomposite film decreases the level of lowest Ge concentration. The SEM image of W-Ge nanocomposite films at 40% Ge concentration shows a smoother surface profile (Figure 2d). As expected from the SEM image given in Figure 2e, the 60% Ge concentration leads to the highest surface roughness due to high number of grains and pores.

The effect of the variation of Ge concentration on surface

wetting characteristic was determined by measuring contact angle values 60 s after dropping  $1\mu\text{l}$  distilled water on thin film surface and the results are illustrated in Figure 3b. The wetting property of a surface is defined as hydrophobic if the contact angle is greater than  $90^\circ$  and hydrophilic if it is less than  $90^\circ$  (Law 2014; Kuruoğlu 2022). The contact angle values of W-Ge nanocomposite coatings with 5%, 10%, 20%, 40% and 60% Ge concentration are  $68^\circ.6$ ,  $55^\circ.8$ ,  $27^\circ.4$ ,  $85^\circ.6$  and  $62^\circ.7$ , respectively. Hence, as shown in Figure 3b, the W-Ge nanocomposite coatings altered with Ge concentration have hydrophilic surfaces and the highest and the lowest contact angle values are obtained at 40% and 20% Ge concentrations, respectively. Additionally, the contact angle values of the remaining Ge concentrations are apparently similar. It is well known that surface chemistry and surface morphology determine the wetting characteristic of surface. The effect of surface morphology (smooth or rough surface) on the wettability of surface were modelled by Young (1805) and Cassie & Baxter (1944) or Wenzel (1936). According to the Wenzel model, an increase in roughness leads to a hydrophilic surface to be more hydrophilic, and a hydrophobic surface to be more hydrophobic. The results of surface roughness measurements and wettability tests of W-Ge nanocomposite films reveal that, in general, with the increase of surface roughness, the wettability of the surfaces decreases (see Figure 3a-b). It can be concluded that W-Ge nanocomposite films have hydrophilic surface properties and their hydrophilicity increases with increasing surface roughness, which obeying Wenzel model (Wenzel 1936). While, W-Ge nanocomposite films with 60% Ge concentration possess the highest rms surface roughness value of 93.3 nm, its contact angle ( $62^\circ.7$ ) is approximately the same values of W-Ge nanocomposite coatings with 5% Ge concentration. This behaviour can be explained with Cassie-Baxter model where droplet cannot penetrate the surface cavities, regardless to the nature of surface, owing to the air pockets under the droplet (Foadi et al. 2019b,a).

Gram-positive (*Staphylococcus aureus* 6538 P., *Bacillus subtilis* IM 622) and gram-negative (*Salmonella typhimurium* NR-RLE 4413, *Escherichia coli* ATCC 25922) were used as model bacteria to reveal antibacterial activities of the W-Ge based nanocomposite coatings as a function of Ge concentration. The formation of inhibition zones confirms the presence of antibacterial activity in all W-Ge nanocomposite coatings. The antibacterial effects of the coatings on gram-positive and gram-negative bacteria follow different patterns and it is observed that it is more effective against to gram-positive bacteria as presented in Figure 4a-b. These differences can be attributed to the differences in cell wall of bacteria. Gram-positive bacteria has a thick peptidoglycan layer and no outer lipid membrane whilst gram-negative bacteria has a thin peptidoglycan layer and has an outer lipid membrane. In fact, a gram-positive bacterium (i.e. *S. aureus*) is made up of an outer membraneless peptidoglycan layer with a thickness ranging from 20 to 80

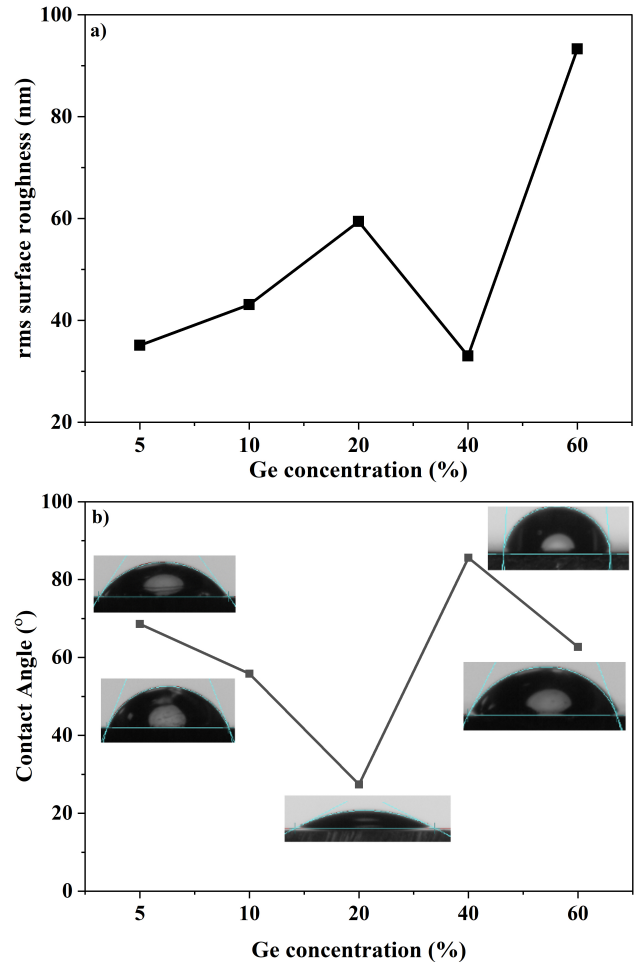


**Figure 3.** a) Surface roughness and b) contact angle values of W-Ge nanocomposite coatings thin film surfaces as a function of Ge concentration.

nm. The outer membrane is an extra layer that *E. coli* has, despite being a gram-negative bacteria with a considerably thinner layer of peptidoglycan (thickness of 78 nm). Additionally, it has been previously noted that the outer membrane of the gram-negative *E. coli* bacterium made *E. coli* more resistant to an AFM tip-induced direct contact interaction than *S. aureus* (Akhavan & Ghaderi 2010; Eaton et al. 2008). Antibacterial efficiencies of W-Ge nanocomposite coatings against to *E. coli* and *S. typhimurium* as a function of Ge concentration show similar behaviour with increasing up to 20% Ge concentration and small amount decrease at 40% Ge. The surface roughness of the coatings is found to play a critical role in their antibacterial efficacy against *S. typhimurium*, and increasing surface roughness led to oxidation of the coatings, resulting in more intense  $\text{GeO}_2$  and  $\text{WO}_3$  peaks rather than metallic W (as shown in Figure 1). These findings are supported by the literature that has revealed the influence of surface roughness and  $\text{WO}_3$  of antibacterial efficiency of the coatings (Wu et al. 2018b,a; Tan et al. 2021). Additionally, while W-Ge nanocomposite coating with 60% Ge concentration exhibits the highest antibacterial effects against *S. typhimurium*, with a high number of grains



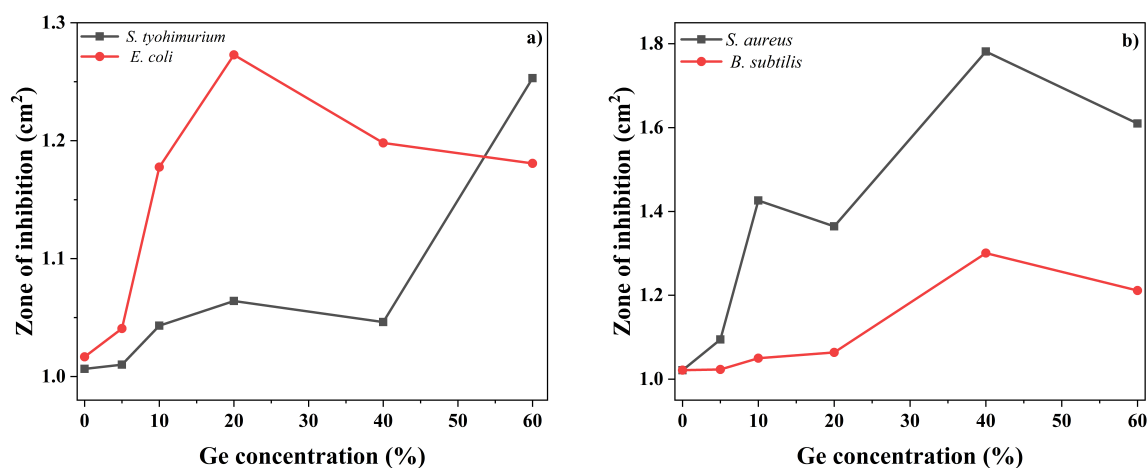


**Figure 4.** Antibacterial activity of W-Ge nanocomposite coatings as function of Ge concentration on a) gram-negative bacteria and b) gram-positive bacteria.

and the most intense WO<sub>3</sub> peaks, a similar effect is observed at 20% Ge concentration against *E. coli* (as shown in Figure 4a). As demonstrated in Figure 4b, the antibacterial efficiency of W-Ge nanocomposite coatings against *S. aureus* and *B. subtilis* is reasonably higher than against the gram-negative bacteria and exhibits the same tendency as a function of Ge concentration, with maximum efficiency being reached at 40% Ge concentration against *S. aureus*.

#### 4. CONCLUSION

In this study, findings on the selective antibacterial properties of W-Ge nanocomposite films based on varying Ge concentrations were presented. With increasing Ge concentration, two types of surface mechanisms (goosefoot and cauliflower-type) were observed, resulting to changes in surface roughness. The study also found that increased surface roughness led to higher oxidation of the coatings due to a higher number of grains. The coatings were found to have hydrophilic surfaces with an opposite trend with surface roughness. Results from antimicrobial activity measurements showed that the coatings had antibacterial activity against both gram-negative and gram-positive bacteria, with higher efficacy against gram-positive bacteria. It could be concluded that increased surface roughness led to higher numbers of grain boundaries, intensifying the metals' oxide phases and improving their antibacterial activity.

**Peer Review:** Externally peer-reviewed.

**Author Contribution:** Conception / Design of study - S.Atasoy, S.Aktas; Data Acquisition - S.Atasoy, Y.K., S.Aktas, F.S., M.S.K., A.A., E.D.; Data Analysis / Interpretation - S.Atasoy, S.Aktas, F.S., A.A.; Drafting Manuscript - S.Atasoy, S.Aktas, F.S., A.A., M.S.K.; Critical Revision of Manuscript - S.Atasoy, S.Aktas, F.S., A.A., A.E.; Final Approval and Accountability - S.Atasoy, S.Aktas, F.S.; Technical or Material Support - F.S., M.S.K.; Supervision - A.E.

**Conflict of Interest:** Authors declared no conflict of interest.

**Financial Disclosure:** Authors declared no financial support.

#### LIST OF AUTHOR ORCIDS

S. Atasoy	<a href="https://orcid.org/0000-0003-0712-7904">https://orcid.org/0000-0003-0712-7904</a>
Y. Kurul	<a href="https://orcid.org/0000-0002-8708-6753">https://orcid.org/0000-0002-8708-6753</a>
S. Aktas	<a href="https://orcid.org/0000-0002-9143-6752">https://orcid.org/0000-0002-9143-6752</a>
F. Sarcan	<a href="https://orcid.org/0000-0002-8860-4321">https://orcid.org/0000-0002-8860-4321</a>
M. S. Kurt	<a href="https://orcid.org/0000-0002-2639-1850">https://orcid.org/0000-0002-2639-1850</a>
A. Ayna	<a href="https://orcid.org/0000-0001-6801-6242">https://orcid.org/0000-0001-6801-6242</a>
E. Darendelioğlu	<a href="https://orcid.org/0000-0002-0630-4086">https://orcid.org/0000-0002-0630-4086</a>
A. Erol	<a href="https://orcid.org/0000-0003-4196-1791">https://orcid.org/0000-0003-4196-1791</a>

#### REFERENCES

- Akhavan O., Ghaderi E., 2010, *ACS Nano*, 4, 5731
- Arslan M. E., Kurt M. Ş., Aslan N., Kadi A., Öner S., Çobanoğlu Ş., Yazici A., 2022, *Journal of Biomedical Materials Research Part B: Applied Biomaterials*, 110, 1667
- Bian D., et al., 2017, *Acta Biomaterialia*, 64, 421
- Cassie A. B. D., Baxter S., 1944, *Trans. Faraday Soc.*, 40, 546
- Chuang K.-T., Abdullah H., Leu S.-J., Cheng K.-B., Kuo D.-H., Chen H.-C., Chien J.-H., Hu W.-T., 2017, *Journal of Photochemistry and Photobiology A: Chemistry*, 337, 151
- Eaton P., Fernandes J. C., Pereira E., Pintado M. E., Xavier Malcata F., 2008, *Ultramicroscopy*, 108, 1128
- Foadi F., Vaez Allaei S. M., Palasantzas G., Mohammadzadeh M. R., 2019a, *Phys. Rev. E*, 100, 022804
- Foadi F., ten Brink G. H., Mohammadzadeh M. R., Palasantzas G., 2019b, *Journal of Applied Physics*, 125
- Helmerson U., Lattemann M., Bohlmark J., Ehiasarian A. P., Gudmundsson J. T., 2006, *Thin Solid Films*, 513, 1
- Jena G., Anandkumar B., Vanithakumari S., George R., Philip J., Amarendra G., 2020, *Progress in Organic Coatings*, 139, 105444

- Kaplan B. J., Parish W. W., Andrus G. M., Simpson J. S. A., Field C. J., 2004, [The Journal of Alternative and Complementary Medicine](#), 10, 337
- Khalid A. Q., AlJohny B. O., Wainwright M., 2014, [African Journal of Microbiology Research](#), 8, 1080
- Kurt M. Ş., Arslan M. E., Yazici A., Mudu İ., Arslan E., 2021, [Journal of Materials Science: Materials in Medicine](#), 32, 6
- Kuruoğlu F., 2022, [Microfluidics and Nanofluidics](#), 26, 72
- Law K.-Y., 2014, [The Journal of Physical Chemistry Letters](#), 5, 686
- Lück B. E., Mann H., Melzer H., Dunemann L., Begerow J., 1999, [Nephrology Dialysis Transplantation](#), 14, 2464
- Martin P. M., 2009, *Handbook of Deposition Technologies for Films and Coatings: Science, Applications and Technology*. William Andrew
- Menazea A., Awwad N. S., 2020, [Journal of Materials Research and Technology](#), 9, 9434
- Nagata N., Yoneyama T., Yanagida K., Ushio K., Yanagihara S., Matsubara O., Eishi Y., 1985, [The Journal of Toxicological Sciences](#), 10, 333
- Okada K., Okagawa K., Kawakami K., et al. 1989, *Clinical Nephrology*, 31, 219
- Park S.-M., Ikegami T., Ebihara K., Shin P.-K., 2006, [Applied Surface Science](#), 253, 1522
- Roy D., Halder N., Chowdhury T., Chattaraj A., Roy P., 2015, [IOSR J VLSI Signal Process](#), 5, 69
- Sarcan F., 2020, [Nanotechnology](#), 31, 435502
- Sellappa S., Jeyaraman V., 2011, [International Journal of Pharma and Bio Sciences](#), 2, 854
- Somogyvári Z., Langer G., Erdélyi G., Balázs L., 2012, [Vacuum](#), 86, 1979
- Tan G.-L., Tang D., Dastan D., Jafari A., Shi Z., Chu Q.-Q., Silva J. P., Yin X.-T., 2021, [Ceramics International](#), 47, 17153
- Voevodin A. A., O'Neill J. P., Prasad S. V., Zabinski J. S., 1999, [Journal of Vacuum Science & Technology A](#), 17, 986
- Wenzel R. N., 1936, [Industrial & Engineering Chemistry](#), 28, 988
- Wu S., Altenried S., Zogg A., Zuber F., Maniura-Weber K., Ren Q., 2018a, [ACS Omega](#), 3, 6456
- Wu S., Zuber F., Maniura-Weber K., Brugger J., Ren Q., 2018b, [Journal of Nanobiotechnology](#), 16, 20
- Young T., 1805, [Philosophical Transactions of the Royal Society of London](#), 95, 65
- Zboun M., Arisan V., Topcuoglu N., Kuruoglu F., Sener L. T., Sarcan F., 2020, [Surfaces and Interfaces](#), 21, 100703